Control of Cardiac Mitochondrial Fuel Selection by Calcium

Sunil M. Kandel[1], Santosh K. Dasika[1], Ranjan K. Dash[2], Daniel A. Beard[1]

Running title: *Control of Cardiac Mitochondrial Fuel Selection by Calcium*

[1] Department of Molecular and Integrated Physiology, University of Michigan, Ann Arbor MI

[2]Department of Biomedical Engineering, Medical College of Wisconsin, Milwaukee, WI

To whom correspondence should be addressed: Daniel A. Beard, Molecular and Integrative Physiology, University of Michigan, 2800 Plymouth Road, Ann Arbor, MI 48109, Telephone: (734) 736-8040, E-mail: beardda@umich.edu

Keywords: bioenergetics, calcium, carbohydrate metabolism, fatty acid metabolism, mitochondria

Abstract

Calcium ion concentration modulates the function of several mitochondrial enzymes. Specifically, the kinetic operations of the decarboxylating dehydrogenases pyruvate dehydrogenase, isocitrate dehydrogenase, α-ketoglutarate dehydrogenase are all affected by [Ca^{2+}]. Previous studies have shown that, despite its ability to affect the function of specific dehydrogenases, [Ca^{2+}] does not substantially alter mitochondrial ATP synthesis in vitro or in vivo in the heart. We hypothesize that, rather than contributing to respiratory control, [Ca^{2+}] plays a role in contributing to fuel selection. Specifically, cardiac mitochondria are able to use different primary carbon substrates (carbohydrates, fatty acids, and ketones) to synthesize ATP aerobically in the living cells. To determine if and how [Ca^{2+}] affects the relative use of carbohydrates versus fatty acids in vitro we measured oxygen consumption and TCA cycle intermediate concentrations in suspensions of cardiac mitochondria with different combinations of pyruvate and palmitoyl-L-carnitine in the media at various [Ca^{2+}] and ADP infusion rates.

Stoichiometric analysis of the data reveals that when both fatty acid and carbohydrate substrates are available, fuel selection is sensitive to both the rate of ADP infusion and to the calcium concentration. Under low-ATP demand conditions and with zero added Ca^{2+}, β-oxidation provides roughly 70% of acetyl-CoA for the citrate synthase reaction, with the rest coming from the pyruvate dehydrogenase reaction. With increasing both the rate of oxidative ATP synthesis and [Ca^{2+}], the fuel utilization ratio shifts to increased fractional consumption of pyruvate. The effects of ATP synthesis rate and [Ca^{2+}] are shown to be interdependent.

Introduction

The kinetic function of several key enzymes involved in energy metabolism is affected by calcium-dependent processes. These include cytosolic enzymes, such as phosphofructokinase (PFK), for which calcium-calmodulin-dependent oligomerization of the enzyme affects catalytic activity [1, 2], as well as several dehydrogenases present in the mitochondrial matrix [3-5]. It has been proposed that in the myocardium in vivo, ATP, ADP, and inorganic phosphate (Pi) levels are maintained at essentially constant levels at different cardiac work rates because varying ATP consumption rates are balanced by calcium-dependent changes in ATP production rate [3, 6]. This hypothesis, that ATP supply is matched to ATP demand based on an open-loop control system (mediated via mitochondrial Ca^{2+}) lacking a closed-loop feedback control mechanism, is broadly invoked [4, 6]. Yet this open-loop Ca^{2+} activation hypothesis has some important shortcomings. The first concern is that open-loop control systems are inherently unstable to environmental changes and external perturbations. For open-loop stimulation (such as via Ca^{2+}) to represent the sole mechanism controlling myocardial ATP production, the relationship between ATP utilization rate and the stimulatory signal (i.e., mitochondrial Ca^{2+}) would have to remain exactly invariant under all physiological conditions. Otherwise, since the heart turns over its total ATP pool several times per minute, even slight mismatches between supply and demand would be disastrous.

Thus some degree of closed-loop feedback control is needed to maintain cellular ATP concentration at different levels of ATP hydrolysis. It is impossible for open-loop Ca^{2+} hypothesis—on its own—to explain respiratory control in vivo. Indeed, the alternative to the open-loop Ca^{2+} hypothesis is that respiratory con-

trol exerted by feedback of ATP hydrolysis products, introduced by Chance and Williams [7], who concluded that "ADP, and not the inorganic phosphate level, controls the respiration rate." Their conclusions were later supported by in vivo measurements made on skeletal muscle in the 1980's in the Chance lab [8, 9]. Numerous experimental and theoretical studies have supported the feedback hypothesis in the context of skeletal muscle (e.g., [10-13]). Similarly, in the heart the concentrations of ATP hydrolysis products increase with ATP demand in the myocardium in vivo [14-21], in agreement with the feedback hypothesis and providing additional evidence against the open-loop Ca^{2+} hypothesis. Furthermore, our analyses suggest that a key difference between how oxidative ATP synthesis is controlled in skeletal versus cardiac muscle is that in the heart inorganic phosphate and not ADP controls the respiration rate [19-24].

The final difficulty with the open-loop Ca^{2+} hypothesis is that, while Ca^{2+} can be shown to stimulate respiration in vitro under certain conditions, under physiological substrate conditions the effects of Ca^{2+} on oxidative ATP synthesis in vitro are miniscule to modest. Panov and Scaduto [25] showed that with pyruvate and acetyl-carnitine as substrates, Ca^{2+} stimulates a maximal 3-8% increase in the apparent V_{max} and a 10-18% reduction in the apparent K_m for ADP for ATP synthesis. Wan et al. [26] reported a similarly small magnitude of effect of Ca^{2+} with pyruvate as substrate. Vinnakota et al. [27, 28] reported increases in the apparent V_{max} of oxidative phosphorylation of cardiac mitochondria of approximately 15-25% when external free [Ca^{2+}] was raised from 0 to 350 nM. These relatively modest effects are insignificant compared to the 400% increase in ATP synthesis associated with the transition from resting to maximal work in the heart in vivo. While the open-loop Ca^{2+} mechanism may be at work in vivo, its role in stimulating ATP synthesis in vivo may be minor compared to other mechanisms that must be at work [24].

Yet there is growing evidence that normal mitochondrial calcium handling is required for normal cardiac mitochondrial metabolic function. Inducible knockouts of cardiac mitochondrial calcium uniporter function have demonstrated that inhibition of calcium uptake has an inhibitory effect on ATP production in acute stress responses [29, 30]. If Ca^{2+} does not play a major role in matching the steady-state oxidative ATP synthesis rate to ATP demand in the heart in vivo, what might be the physiological function of the sensitivity of pyruvate dehydrogenase, isocitrate dehydrogenase, and α-ketoglutarate dehydrogenase? We hypothesize that Ca^{2+}-mediated effects on these enzymes are involved in substrate selection. Under resting conditions (in the fasted state), roughly 60% of acetyl-CoA supply to the tricarboxylic acid cycle is derived from β-oxidation of fatty acids, with the remaining 40% derived from carbohydrate sources in the heart [31]. In exercise (high ATP demand) conditions the ratio flips, with the majority of acetyl-CoA supplied from oxidation of carbohydrates [31, 32]. This phenomenon of increasing relative contribution from carbohydrate oxidation with increasing ATP synthesis rate is recapitulated in vitro in isolated mitochondria from skeletal muscle [33].

The goals of this study are to: (1.) determine if, similar to what is observed with skeletal muscle mitochondria, changes in ATP synthesis rate cause changes in fuel selection in vitro in suspensions of mammalian cardiac mitochondria; (2.) determine if changes in Ca^{2+} concentration cause changes in fuel selection in vitro; (3.) determine if and how work load and calcium independently and dependently influence mitochondrial substrate selection in vitro; and (4.) to test the hypothesis that increases in mitochondrial Ca^{2+} contribute to a shift to using relatively more carbohydrate and relatively less fatty acid substrate to fuel oxidative ATP synthesis in cardiac mitochondria as ATP synthesis rate is increased. To achieve these goals we measured oxygen consumption and bulk metabolite concentration changes during leak state (state 2 respiration) and during active oxidative phosphorylation (OXPHOS), with carbohydrate, fatty acid, and mixed (carbohydrate + fatty acid) substrates in suspensions of purified rat ventricular mitochondria. Data were analyzed using a quasi-steady-state mass balance approach to estimate TCA cycle fluxes and fractional fuel utilization under different calcium conditions and at different rates of ATP synthesis.

We find that under mixed substrate conditions fuel utilization is modulated in cardiac mitochondria in vitro by both ATP synthesis/demand rate, and by buffer Ca^{2+} concentration. At nominally zero [Ca^{2+}], approximately 30% of acetyl-CoA is supplied to the TCA cycle from pyruvate oxidation, with the rest supplied via β-oxidation. At zero [Ca^{2+}] we are not able to detect a significant dependency of the fuel utilization ratio on ATP synthesis/demand rate. When Ca^{2+} is added to the buffer, at concentrations in the range of 100 to 200 nM free [Ca^{2+}], the contribution from pyruvate becomes dependent on the ATP synthesis/demand rate. With Ca^{2+} present, the fractional contribution from pyruvate is approximately 35-40% at low ATP synthesis/demand levels (corresponding to roughly 1/3 of the apparent V_{max} of oxidative phos-

phorylation) and roughly 50% at high ATP synthesis/demand levels (corresponding to roughly 1/2 of the apparent V_{max} of oxidative phosphorylation). Thus, fuel selection in vitro is shown to depend on both Ca^{2+} level and ATP synthesis/demand rate.

Results

Oxygen consumption rate, and concentrations of several tricarboxylic acid (TCA) cycle metabolites were measured in suspensions of purified rat ventricular mitochondria in the leak state (with substrate present but with no ADP available as a substrate for oxidative phosphorylation), and under conditions of steady ADP infusion to establish a steady rate of ATP production. These data were used to estimate steady-state substrate oxidation and TCA cycle fluxes under different substrate conditions, different Ca^{2+} concentrations, and different rates of oxidative ATP synthesis.

Oxygen consumption rates

Fig. 1A shows representative traces of oxygen consumption flux (J_{O2}) in the leak state ($t < 0$ sec.), during low-rate ADP infusion ($I = 78.9$ nmol ADP·min^{-1}·(ml)$^{-1}$, during $0 < t < 190$ sec.), and after stopping ADP infusion ($t > 190$ sec.). In this and all other experiments, mitochondrial were added at 0.67 units of citrate synthase activity to 2 ml of experimental buffer. Thus, expressing the ADP infusion rate (equal to ATP synthesis rate) relative to mitochondrial citrate synthase activity, $I = 234$ nmol·min^{-1}·(U CS)$^{-1}$ for the low ADP infusion rate case. Representative traces of J_{O2} are shown for three different substrate conditions PYR (pyruvate and malate at initial concentrations of 350 μM and 2 mM), PC (palmitoyl carnitine and malate at initial concentrations of 20 μM and 2 mM), and MIX (pyruvate, palmitoyl carnitine, and malate at initial concentrations of 350 μM, 20 μM and 2 mM, respectively). Fig. 1B shows similar traces, obtained in the leak state ($t < 0$ sec.), during high rate of ADP infusion ($I = 356$ nmol·min^{-1}·(U CS)$^{-1}$, $0 < t < 125$ sec.), and after stopping ADP infusion ($t > 125$ sec.). These two ADP infusion rates correspond to roughly 1/3 and 1/2 of the V_{max} of mitochondrial ATP synthesis in vitro.

Observations from N = 4-6 biological replicates of steady-state J_{O2} during ATP synthesis (OXPHOS state) and at three different Ca^{2+} concentrations are summarized in Figs. 1C and 1D. As expected, the J_{O2} is higher when fatty the acid substrate (PC) is oxidized compared to carbohydrate (PM), although the observed differences are not statistically significant. Oxygen flux tends to increase with increasing Ca^{2+}, possibly due to increased Ca^{2+} cycling contributing to the effective leak flux. The estimated effective P/O ratios under the different calcium and substrate conditions are listed in Table 1. Again, while the differences in P/O ratio under different substrate conditions are not statistically significant, the expected trend of lower P/O ratio with PC compared to PM is observed. Unexpectedly, the P/O ratio tends to be lowest for any given ATP-synthesis/ADP-infusion rate with the mixed substrate.

Even if these small differences were statistically significant, these measurements on their own would not provide enough information to quantify the substrate oxidation and TCA cycle fluxes under the different experimental conditions. To do so, additional data on metabolite concentrations were obtained that, combined with the oxygen flux data, allow us to estimate quasi-steady-state fluxes.

Metabolite concentrations

The purified mitochondria system was quenched and extracted for assay of intermediate concentrations at five different time points in the protocol detailed above and summarized in Fig. 1. For the low ADP infusion rate experiments ($I = 234$ nmol·min^{-1}·(U CS)$^{-1}$) measurements were made at time points 10 and 100 sec. following substrate addition (during the leak state) and at 120, 150, and 180 sec. during the ADP-infusion OXPHOS state. For the high ADP infusion rate experiments ($I = 356$ nmol·min^{-1}·(U CS)$^{-1}$) measurements were made at time points 10 and 110 sec. following substrate addition for the leak state and at 60, 90, and 120 sec. during the ADP-infusion OXPHOS state. Representative data on pyruvate and α-ketoglutarate from these experiments are shown in Figs. 2, 3, and 4.

Fig. 2 shows data obtained using pyruvate + malate (PM) as the substrate, and at 0 added Ca^{2+}, for both ADP infusion rates. Under these conditions, with $I = 234$ nmol·min^{-1}·(U CS)$^{-1}$ roughly 50 μM of pyruvate is consumed and 40 μM of α-ketoglutarate is produced over the 200 second ADP infusion time period. Thus the TCA cycle flux from citrate to α-ketoglutarate is several times higher than the α-ketoglutarate dehydrogenase flux. Most of the carbon entering the TCA cycle as citrate is exiting as α-ketoglutarate, rather than continuing on to complete the cycle and resynthesize citrate from oxaloacetate. Rather, as has been observed previously, the exogenous malate consumed via malate dehydrogenase is the primary source of oxaloacetate for the citrate synthase reaction under these conditions [34]. A similar phenomenon is observed at the higher ADP infusion rate. Furthermore, similar results are obtained at different Ca^{2+} concentrations, as shown in the Supplemental Data (Figs. S1 and S2).

Under mixed substrate conditions (MIX), the pyruvate consumption rate is much lower than observed with pyruvate + malate substrate. Fig. 3 shows data for the high Ca^{2+} case. (Results for other Ca^{2+} concentrations are shown in Figs. S3 and S4 of the Supplemental Data.) Although the pyruvate consumption rates are lower, the α-ketoglutarate production rates are similar to those observed under the pyruvate + malate (PM) substrate conditions, indicating that a similarly low fraction of the citrate to α-ketoglutarate flux is continuing on to complete the cycle through the α-ketoglutarate dehydrogenase, succinyl-CoA synthetase, succinate dehydrogenase, and fumarase reactions.

Under the PC substrate conditions (palmitoyl-carnitine + malate) no pyruvate consumption or production is observed (Fig. 4 and Figs. S5 and S6), with α-ketoglutarate production similar to that observed under the other substrate conditions.

Quasi-steady state flux analysis

In total, oxygen consumption rate and metabolite intermediate concentrations were assayed under 27 different experimental conditions: (leak state + 2 OXPHOS states) × (3 Ca^{2+} conditions) × (3 substrate conditions). Under these different conditions, citrate, succinate, fumarate, and oxaloacetate were observed to all remain below the limit of detection (approximately 15 μM) of the assays employed. Based on this observation we constructed a reduced stoichiometric mass conservation model illustrated in Fig. 5, in which the fluxes J_1 (rate of acetyl-CoA production from pyruvate dehydrogenase), J_2 (rate of α-ketoglutarate production), J_3 (rate of succinate dehydrogenase/complex II flux), and J_4 (rate of acetyl-CoA production from β-oxidation) are unknowns to be estimated based on the metabolite and oxygen flux data at each experiments condition. (The flux J_3 is assumed equal to $J_1 + J_4 - J_2$ under steady state conditions.) Thus, under each steady-state condition, there are three unknown steady-state fluxes, J_1, J_2, and J_4 to be estimated from data on oxygen consumption rate and metabolite concentrations. We use the notation $J_1^{(2)}$, $J_2^{(2)}$, and $J_4^{(2)}$ to represent fluxes in the state-2 (leak) state, and $J_1^{(3)}$, $J_2^{(3)}$, and $J_4^{(3)}$ to represent fluxes in the state-3 (OXPHOS) state. In all states, the oxygen consumption flux is stoichiometrically equated to half of the rate of generation of electron donors (NADH, $FADH_2$, QH_2):

$$J_{O_2} = \frac{1}{2}(5J_1 + 6J_4 - 2J_2).$$

For conditions with pyruvate + malate (PM) substrate, $J_4 = 0$, and we have the following equations for the leak state

$$\begin{aligned} J_{O2}^{(2)} &= \tfrac{1}{2}\left(5J_1^{(2)} - 2J_2^{(2)}\right) \\ C_{PYR}(t) &= C_{0,PYR} - J_1^{(2)}t, \\ C_{AKG}(t) &= C_{0,AKG} + J_2^{(2)}t, \qquad t < T \quad (1) \end{aligned}$$

where $C_{PYR}(t)$ and $C_{AKG}(t)$ are the concentrations of pyruvate and α-ketoglutarate, $C_{0,PYR}$ and $C_{0,AKG}$ are the initial concentrations, and $T = 0$ is the time of the beginning of ADP infusion. These equations assume a linear consumption of pyruvate, linear production of α-ketoglutarate, and a constant rate of oxygen consumption.

The equations for the OXPHOS state, which is initiated at $t = T$ are

$$\begin{aligned} J_{O2}^{(3)} &= \tfrac{1}{2}\left(5J_1^{(3)} - 2J_2^{(3)}\right) \\ C_{PYR}(t) &= C_{0,PYR} - J_1^{(2)}T - J_1^{(3)}t \\ C_{AKG}(t) &= C_{0,AKG} + J_2^{(2)}T + J_2^{(2)}t, \quad t \geq T. \end{aligned} \quad (2)$$

These equations assume a piecewise linear time course of pyruvate and α-ketoglutarate, as illustrated in Figs. 2-4.

For experiments with PM substrate (at three different $[Ca^{2+}]$ concentrations and two different ADP infusion rates for the OXPHOS state), Equations (1) and (2) are fit to experimental data on $C_{PYR}(t)$, $C_{AKG}(t)$, $J_{O2}^{(2)}$, and $J_{O2}^{(3)}$ to obtain estimates of unknowns $J_1^{(2)}$, $J_2^{(2)}$, $J_1^{(3)}$, $J_2^{(3)}$, $C_{0,PYR}$, and $C_{0,AKG}$. Even though we set initial pyruvate and α-ketoglutarate at 350 and 0 μM in the experiments, we allow $C_{0,PYR}$, and $C_{0,AKG}$ to be estimated in order to account for experimental variability and contamination in sample prep.

For palmitoyl-carnitine (PC) substrate, the equations become

$$\begin{aligned} J_{O2}^{(2)} &= \tfrac{1}{2}\left(6J_4^{(2)} - 2J_2^{(2)}\right) \\ C_{PYR}(t) &= C_{0,PYR} \\ C_{AKG}(t) &= C_{0,AKG} + J_2^{(2)}t, \qquad t < T \quad (3) \\ J_{O2}^{(3)} &= \tfrac{1}{2}\left(6J_4^{(3)} - 2J_2^{(3)}\right) \\ C_{AKG}(t) &= C_{0,AKG} + J_2^{(2)}T + J_2^{(3)}t, \quad t \geq T, \end{aligned} \quad (4)$$

where the unknowns are $J_2^{(2)}, J_4^{(2)}, J_2^{(3)}, J_4^{(3)}, C_{0,PYR}$, and $C_{0,AKG}$.

With mixed substrate (MIX), the governing equations are

$$\begin{aligned} J_{O2}^{(2)} &= \tfrac{1}{2}\left(5J_1^{(2)} + 6J_4^{(2)} - 2J_2^{(2)}\right) \\ C_{PYR}(t) &= C_{0,PYR} - J_1^{(2)}t, \\ C_{AKG}(t) &= C_{0,AKG} + J_2^{(2)}t, \qquad t < T \end{aligned} \tag{5}$$

and

$$\begin{aligned} J_{O2}^{(3)} &= \tfrac{1}{2}\left(5J_1^{(3)} + 6J_4^{(3)} - 2J_2^{(3)}\right) \\ C_{PYR}(t) &= C_{0,PYR} - J_1^{(2)}T - J_1^{(3)}t \\ C_{AKG}(t) &= C_{0,AKG} + J_2^{(2)}T + J_2^{(3)}t, \quad t \geq T, \end{aligned} \tag{6}$$

and the unknowns are $J_1^{(2)}, J_2^{(2)}, J_4^{(2)}, J_1^{(3)}, J_2^{(3)}, J_4^{(3)}$, $C_{0,PYR}$, and $C_{0,AKG}$.

For each substrate and Ca^{2+} condition, maximal likelihood estimates for the unknowns and for the covariances among the unknowns are obtained using the methods of Landaw and DiStefano [35]. The goodness of fit to the data and uncertainty in flux estimates are evaluated using Monte-Carlo sampling from the distributions associated with the maximally likely means and covariances for the estimated unknowns from the governing equations. For a given substrate and Ca^{2+} condition an individual estimate of the unknown fluxes and initial conditions yields piecewise linear fits to the pyruvate and α-ketoglutarate data and pointwise estimates of J_{O2} for the leak state and the two OXPHOS states. By drawing 1000 samples from the flux and initial condition distributions for each substrate and Ca^{2+} condition, we estimate the uncertainties in the estimates of the unknowns.

Fuel selection in vitro

Table 2 lists the estimated fluxes and uncertainties for each condition. Uncertainties are indicated as ± 1 SD confidence range. The estimates for J_{O2} in Table 2, which arise from the fits of the appropriate set of governing equation to the data, can be compared directly to the direct measurements in Table 1. The close correspondence between the measurements in Table 1 and the estimates in Table 2 (that are based on fitting both the data in Table 1 and the concentration data) provides an independent validation of the steady-state analysis.

Representative piecewise linear fits to the concentration data are shown in Fig. 2 (PM substrate, $[Ca^{2+}] = 0$), Fig. 3 (MIX substrate, $[Ca^{2+}] = 400$ μM), and Fig. 4 (PC substrate, $[Ca^{2+}] = 300$ μM). Plots for all other conditions are show in Figs. S1 to S6 of the Supplemental Data. For clarity of presentation only 25 of the 1000 independent fits are shown. The piecewise linear steady-state model effectively matches the data, and the Monte-Carlo sampling effectively matches to the uncertainty in the data, illustrated as mean ± SEM. The flux estimates shown in Table 2 for mixed substrate conditions are used to estimate the fractional utilization of carbohydrate versus fatty acid under different OXPHOS loads and Ca^{2+} concentrations. The estimated flux values are for the high-demand (I = 356 nmol min^{-1} $(UCS)^{-1}$) case are show in Fig. 6. For this demand level at $[Ca^{2+}] = 0$, β-oxidation provides roughly 70% of acetyl-CoA for the citrate synthase reaction, with approximately 30% from the pyruvate dehydrogenase reaction. At the higher levels of $[Ca^{2+}]$, the substrate utilization ratio becomes approximately 1:1.

Estimated fuel utilization fractions are plotted in Figs. 7 and 8. At $[Ca^{2+}] = 0$ the fatty acid:carbohydrate ratio is approximately 70:30, regardless of ATP demand level. A trend of increasing fractional pyurvate utilization with increasing calcium is observed at both demand levels (Fig. 7). The magnitude of the relationship is greater at the higher demand level but does not reach statistical significance for either the low-demand ($p = 0.28$) or high-demand ($p = 0.19$) case. Combining the data at both demand rates, the fractional utilization of pyruvate is 0.298 ± 0.096 at zero Ca^{2+}. For the low-demand case, combining data from both non-zero calcium levels, the estimated fractional utilization of pyruvate is 0.373 ± 0.105. For the high-demand non-zero calcium case the fractional utilization of pyruvate increase to 0.475 ± 0.134. The observed differences in fractional utilization of pyruvate, comparing the 0-calcium and non-zero calcium cases, are statistically insignificant ($p = 0.14$) for the low-demand case, and statistically significant ($p = 0.014$) for the high-demand case.

Thus we can conclude that fractional substrate utilization is dependent on both calcium and ATP demand rate. Both increasing calcium and increasing demand rate cause an apparent increase in fractional utilization of pyruvate. The observed differences become statistically significant only when the high-demand non-zero calcium case is compared to the low-calcium cases.

Estimated leak current

The contributions of leak current to the overall oxidative flux may be estimated for the various experimental conditions probed based on the flux estimates reported in Table 2. These calculations are based on the following stoichiometric assumptions: (1.) each Complex I donor (NADH) generated is associated with 10 charges pumped across the inner membrane; (2.) each Complex II donor ($FADH_2$ and QH_2) generated is associated with 6 charged pumped; (3.) Each ATP generated is associated with a current of 11/3 charges. The 11/3 stoichiometric coefficient for ATP generation assumes an 8/3 stoichiometry for the ATPase [36], and 1 charge transferred by the adenine nucleotide translocase. Computing leak current (J_L) as the difference between the total rate of charge pumping via the respiratory chain and the rate of charge consumption for ATP synthesis, we have

$$J_L = 46J_1 + 52J_4 - 16J_2 - (11/3)I.$$

Values of J_L estimated using these assumptions are plotted in Fig. 9. This current is expected to be primarily composed of H^+ ions, with secondary contributions associated with calcium cycling and other currents. In the leak state ($I = 0$), the estimated leak currents are approximately 400 nmol·min^{-1}·(U CS)$^{-1}$. Since slightly fewer than 20 charges are pumped by the respiratory complexes per O_2 molecule consumed, the leak current in the leak state may be alternatively estimated as slightly less than 20 times J_{O2} under pyruvate substrate conditions. Indeed, 20 times the average leak state J_{O2} with pyruvate substrate is 358 nmol·min^{-1}·(U CS)$^{-1}$. As demand is increased ($I = 234$ and 356 nmol·min^{-1}·(U CS)$^{-1}$), the estimated leak current decreases, presumably due to a decrease in magnitude of the mitochondrial membrane potential. Under OXPHOS conditions J_L is estimated to be approximately 200-300 nmol·min^{-1}·(U CS)$^{-1}$. Since the ATP-producing current is 11/3 times I, the ratios of ATP-producing current to leak current are approximately 3:1 at $I = 1/3$ of V_{max}, and 7:1 at $I = 1/2$ of V_{max}.

The estimates in Fig. 9 do not show any clearly discernable dependency of J_L on Ca^{2+} concentration. Thus we are not able to estimate the small contribution of calcium current [37, 38] to the overall leak current.

Discussion

This study was designed to determine if and how fuel selection in vitro in cardiac mitochondria is affected by ATP demand and Ca^{2+} concentration, and to test the specific hypothesis that increases in mitochondrial Ca^{2+} can cause a shift to using relatively more carbohydrate and relatively less fatty acid substrate to fuel oxidative ATP synthesis in cardiac mitochondria.

Our results demonstrate a modest dependency of fuel selection on ATP demand. In the presence of nonzero calcium, the relative contribution of pyruvate to oxidative metabolism in mixed substrate conditions increases from 37.3 ±10.5% at the ADP infusion rate of I = 234 nmol·min^{-1}·(U CS)$^{-1}$ (approximately 1/3 of V_{max}) to 47.5 ± 13.4% at I = 356 nmol·min^{-1}·(U CS)$^{-1}$ (approximately 1/2 of V_{max}). Although the uncertainty in these estimates is relatively high, the difference between the high-demand/non-zero calcium case and the low calcium cases is statistically significant. These findings may be compared to the trend of increasing fraction al pyruvate utilization with increasing demand observed by Kuzmiak-Glancy and Willis [33] in skeletal muscle mitochondrial from rat and sparrow.

The trend of increasing relative contribution of pyruvate with increasing ATP demand is apparent at all Ca^{2+} concentrations. However, the magnitude of the trend increases with [Ca^{2+}] and becomes statistically significant only for nonzero [Ca^{2+}]. Thus, the effects of Ca^{2+} on mitochondrial fuel selection in vitro are dependent on ATP demand level. The effects of Ca^{2+} and increasing ATP demand on substrate switching appear to be additive. Furthermore, our data suggest that, at least under the in vitro conditions probed in this study, the primarily regulator of Ca^{2+}-dependent fuel selection is pyruvate dehydrogenase. Flux through downstream dehydrogenases does not show clear dependencies on Ca^{2+} concentration under any of the substrates employed here.

Based on these observations we speculate that a physiological non-zero calcium concentration is necessary for cardiac mitochondria to effectively switch from a low-capacity fuel (fats) to a high-capacity fuel (carbohydrates) in response to acute increases in workload. This mechanism may help explain observations that deletion of the cardiac mitochondrial calcium uniporter is associated with an impaired ability of the heart to acutely match ATP production to demand [29, 30].

Finally, our data provide a means to estimate leak current at the different ATP demand rates assayed in the experiments. Under high-demand OXPHOS conditions the leak current is about half of that estimated for the zero-demand leak state. In our preparation the respiratory coupling efficiency estimated as the ratio of maximally simulated J_{O2} during OXPHOS to the leak state J_{O2} is approximately 8:1. Because the leak current decreases by about a factor of 2 in going from leak state to the OXPHOS state, we can estimate the coupling

efficiency ratio during the maximum rate of ATP synthesis to be approximately 15:1 for the in vitro preparation.

In summary, our results show that a fuel selection switch from fatty acids to greater fractional utilization of pyruvate occurs with increasing ATP demand rate and calcium in cardiac mitochondria in vitro. These results mirror previous observation obtained using isolated skeletal muscle mitochondria [33]. Finally, these observations are consistent with our hypothesis that calcium stimulates the switch to carbohydrate oxidation with increasing ATP demand in vivo.

Experimental Procedures

Isolation of Mitochondria

Cardiac mitochondria were isolated from Male Wistar rats of 300–400 g using protocols that were approved by the Animal Care Committee of the University of Michigan. The rats were anesthetized with an intraperitoneal injection of appropriate amount of ketamine mixed with dexmed, followed by heparin. After the rat was in the deep plane of anesthesia, hearts were excised, the aortas cannulated and hearts perfused with ice-cold cardioplegia buffer (containing 25 mM KCl, 100 mM NaCl, 10 mM Dextrose, 25 mM MOPS, 1 mM EGTA) for a 5-minute period. The ventricles of the excised heart were then immediately placed in ice-cold isolation buffer containing 200 mM mannitol, 50 mM sucrose, 5 mM KH_2PO_4, 5 mM MOPS, 1 mM EGTA, and 0.1% BSA. The ventricles were minced, added to 2.5 ml of a solution of 5 units/ml protease, with sample volume adjusted to 12.5 ml, and homogenized at low speed (position 12-20) for maximum 40 seconds. The isolation buffer was added to the homogenate to a final volume of 25 ml and centrifuged twice at 8000 g for 10 min at 4°C to remove the protease. The supernatant was discarded, and the pellet was resuspended in the isolation buffer to 25 ml and centrifuged at 700 g for 10 min. The pellet was then removed and the supernatant enriched with mitochondria was spun at 8000 g for 10 min. The pellet, representing the mitochondrial-enriched fraction, was resuspended in 0.2 ml of isolation buffer.

To determine the content of intact mitochondria, citrate synthase (CS) activity was assessed as a quantitative marker of the mitochondrial matrix. The enzymatic activity of citrate synthase was assayed following the protocol of Eigentler et al. [39].

Respiratory Control Index

The functional integrity of the mitochondria was determined by means of the respiratory control index defined as the maximum rate of oxygen consumption in state-3 oxidative phosphorylation (OXPHOS) divided by the state-2 (leak) state oxygen consumption rate. Both maximal OXPHOS and leak states were assessed with 5 mM pyruvate and 1 mM malate as substrates at 37° C. The OXPHOS state was assessed with ADP added at initial concentration of 500 μM. Oxygen consumption was determined at 37° C using a high resolution respirometer (Oxygraph-2K-Fluorescence LED2 module, OROBOROS Instruments Gmbh, Innsbruck, Austria). Mitochondria preparations with respiratory control index greater than 8 were considered to be of acceptable quality for our experiment.

Steady ATP Synthesis Experiments

Isolated mitochondria were resuspended in the respiration buffer (80 mM KCl, 10 mmol/l Tris/HCl, 1 mM EDTA, 5 mM KH_2PO_4, pH 7.4). The experiments were conducted with three different substrate combinations: pyruvate + malate (PM), palmitoyl carnitine (PC) + malate, and pyruvate + PC + malate (MIX) with three different $CaCl_2$ concentrations, and two different ADP infusion rates at 37° C and 7.2 pH. The final substrate concentrations were: malate: 2 mM, pyruvate: 350 μM, PC: 20 μM. Total calcium ($CaCl_2$) concentrations were: 0, 300 μM, and 400 μM.

Experimental buffer for a given experimental condition was prepared by adding 20 μl of NaCl (1 M stock) and 8 μl of the either water or $CaCl_2$ (75 or 100 mM stock) 2 ml of the respiration buffer. Experiments were initiated (at time defined 0 seconds) mitochondria and substrates were added, to initiate leak state respiration. After 2 minutes of leak state respiration, 10 μl of 50 mM ADP was infused into the chamber via the electronic controlled titration-injection micropump TIP-2K (a modular component of the Oxygraph) at the rate of 0.0526 μl /sec (low workload) and 0.0800 μl /sec (high workload).

In total, 18 different experimental conditions were studied: for the three different substrate conditions, three different calcium concentrations, and two different ADP infusion rates. For oxygen consumption measurements each experiment was replicated at least 4 times.

Oxygen concentration was recorded throughout these experiments using the Oroboros oxyrgaph (Oroboros).

Mitochondrial Extraction and Metabolite Assays

To measure the accumulation/utilization of various TCA cycle intermediates (pyruvate, α-ketoglutarate, citrate) at various time points, samples were quenched at five different points in the steady-state protocols

(two during the leak state and two during the ADP-infusion OXPHOS state.) Samples were quenched adding 800 µl of the experimental sample to 560 µl of 0.6 M perchloric acid (PCA). The quenched samples were than centrifuged at 15,000 rpm for 10 mins at 4° C. After the centrifugation 1300 µl of the supernatant was collected in a different tube and adjusted the pH to between 7.0 and 7.4. The samples were then centrifuged once again for 10 mins at 15000 rpm at 4° C and 1 ml of the supernatant of the centrifuged samples were collected to measure the concentration of the desired metabolites enzymatically.

For each of the 18 experimental conditions, samples were collected at 10 and 110 seconds during the leak state. For the low workload condition, three samples were collected at times 120, 150, and 180 seconds. For the high workload condition, three samples were collected at times 60, 90 and 120 seconds. For each sample collection time, at least 4 (6 replicates in the mixed sample) replicates were obtained.

Metabolite Assays

Metabolite assays were adapted from the methods of Williamson and Corkey [40]. For all measured metabolites NADH-linked assays were used, where the oxidation/reduction of specific metabolites are linked changes in NADH, monitored by changes in absorbance at 340 nm. Assays were run using neutralized extract in a final assay volume of 1 ml. Standard curves were obtained daily.

The α-ketoglutarate (AKG) concentration was measured by coupling glutamate oxaloacetate transaminase (GOT, EC: 2.6.1.1) with malate dehydrogenase (MDH, EC: 1.1.1.37) and adding excess of aspartate (ASP) to the system and obtaining the difference between NADH concentration before and after adding ASP:

$$\text{ASP} + \text{AKG} + \text{NADH} \rightleftharpoons \text{GLU} + \text{MAL} + \text{NAD}.$$

Pyruvate (PYR) concentration was measured by adding lactate dehydrogenase (LDH, EC: 1.1.1.27) to catalyze PYR reduction and NADH oxidation and by computing the difference in NADH before and after adding LDH:

$$\text{PYR} + \text{NADH} \rightleftharpoons \text{LAC} + \text{NAD}.$$

The enzyme citrate lyase (CL, EC: 4.1.3.6) catalyzes the conversion of citrate (CIT) to oxaloacetate (OAA). Since the OAA produced is readily reduced to malate due the presence of MDH, citrate concentration was estimated by computing the difference between NADH concentration before and after adding CL:

$$\text{CIT} \rightleftharpoons \text{OAA}$$

$$\text{OAA} + \text{NADH} \rightleftharpoons \text{MAL} + \text{NAD}.$$

Acknowledgments

This work supported by NIH grants HL072011 and HL122199.

Conflict of Interest

The authors declare that they have no conflicts of interest with the contents of this article.

Author Contributions

DAB, SMK, and SKD designed the study and wrote the paper. SMK and SKD conducted the experiments and analyzed the data. All authors analyzed the results and approved the final version of the paper.

References

1. Marinho-Carvalho, M.M., et al., *Calmodulin upregulates skeletal muscle 6-phosphofructo-1-kinase reversing the inhibitory effects of allosteric modulators.* Biochim Biophys Acta, 2009. **1794**(8): p. 1175-80.

2. Marinho-Carvalho, M.M., P. Zancan, and M. Sola-Penna, *Modulation of 6-phosphofructo-1-kinase oligomeric equilibrium by calmodulin: formation of active dimers.* Mol Genet Metab, 2006. **87**(3): p. 253-61.

3. Williams, G.S., L. Boyman, and W.J. Lederer, *Mitochondrial calcium and the regulation of metabolism in the heart.* J Mol Cell Cardiol, 2015. **78**: p. 35-45.

4. Griffiths, E.J. and G.A. Rutter, *Mitochondrial calcium as a key regulator of mitochondrial ATP production in mammalian cells.* Biochim Biophys Acta, 2009. **1787**(11): p. 1324-33.

5. Denton, R.M., *Regulation of mitochondrial dehydrogenases by calcium ions.* Biochim Biophys Acta, 2009. **1787**(11): p. 1309-16.

6. Balaban, R.S., *Cardiac energy metabolism homeostasis: role of cytosolic calcium.* J Mol Cell Cardiol, 2002. **34**(10): p. 1259-71.

7. Chance, B. and G.R. Williams, *The respiratory chain and oxidative phosphorylation.* Adv Enzymol Relat Subj Biochem, 1956. **17**: p. 65-134.

8. Chance, B., et al., *Control of oxidative metabolism and oxygen delivery in human skeletal muscle: a steady-state analysis of the work/energy cost transfer function.* Proc Natl Acad Sci U S A, 1985. **82**(24): p. 8384-8.

9. Chance, B., et al., *Multiple controls of oxidative metabolism in living tissues as studied by phosphorus magnetic resonance.* Proc Natl Acad Sci U S A, 1986. **83**(24): p. 9458-62.

10. Kemp, G.J., M. Meyerspeer, and E. Moser, *Absolute quantification of phosphorus metabolite concentrations in human muscle in vivo by 31P MRS: a quantitative review.* NMR Biomed, 2007. **20**(6): p. 555-65.

11. Jeneson, J.A., et al., *The signal transduction function for oxidative phosphorylation is at least second order in ADP.* J Biol Chem, 1996. **271**(45): p. 27995-8.

12. Jeneson, J.A., H.V. Westerhoff, and M.J. Kushmerick, *A metabolic control analysis of kinetic controls in ATP free energy metabolism in contracting skeletal muscle.* Am J Physiol Cell Physiol, 2000. **279**(3): p. C813-32.

13. Kushmerick, M.J., R.A. Meyer, and T.R. Brown, *Regulation of oxygen consumption in fast- and slow-twitch muscle.* Am J Physiol, 1992. **263**(3 Pt 1): p. C598-606.

14. Bache, R.J., et al., *Myocardial oxygenation at high workstates in hearts with left ventricular hypertrophy.* Cardiovasc Res, 1999. **42**(3): p. 616-26.

15. Gong, G., et al., *Oxidative capacity in failing hearts.* Am J Physiol Heart Circ Physiol, 2003. **285**(2): p. H541-8.

16. Gong, G., K. Ugurbil, and J. Zhang, *Transmural metabolic heterogeneity at high cardiac work states.* Am J Physiol, 1999. **277**(1 Pt 2): p. H236-42.

17. Ochiai, K., et al., *Effects of augmented delivery of pyruvate on myocardial high-energy phosphate metabolism at high workstate.* Am J Physiol Heart Circ Physiol, 2001. **281**(4): p. H1823-32.

18. Zhang, J., et al., *Nitric oxide regulation of myocardial O2 consumption and HEP metabolism.* Am J Physiol Heart Circ Physiol, 2005. **288**(1): p. H310-6.

19. Wu, F., et al., *Phosphate metabolite concentrations and ATP hydrolysis potential in normal and ischaemic hearts.* J Physiol, 2008. **586**(17): p. 4193-208.

20. Wu, F., J. Zhang, and D.A. Beard, *Experimentally observed phenomena on cardiac energetics in heart failure emerge from simulations of cardiac metabolism.* Proc Natl Acad Sci U S A, 2009. **106**(17): p. 7143-8.

21. Beard, D.A., *Simulation of cellular biochemical system kinetics.* Wiley Interdiscip Rev Syst Biol Med, 2011. **3**(2): p. 136-46.

22. Wu, F., J.A. Jeneson, and D.A. Beard, *Oxidative ATP synthesis in skeletal muscle is controlled by substrate feedback.* Am J Physiol Cell Physiol, 2007. **292**(1): p. C115-24.

23. Wu, F. and D.A. Beard, *Roles of the creatine kinase system and myoglobin in maintaining energetic state in the working heart.* BMC Syst Biol, 2009. **3**: p. 22.

24. Beard, D.A. and M.J. Kushmerick, *Strong inference for systems biology.* PLoS Comput Biol, 2009. **5**(8): p. e1000459.

25. Panov, A.V. and R.C. Scaduto, Jr., *Substrate specific effects of calcium on metabolism of rat heart mitochondria.* Am J Physiol, 1996. **270**(4 Pt 2): p. H1398-406.

26. Wan, B., et al., *Regulation of citric acid cycle by calcium.* J Biol Chem, 1989. **264**(23): p. 13430-9.

27. Vinnakota, K.C., R.K. Dash, and D.A. Beard, *Stimulatory effects of calcium on respiration and NAD(P)H synthesis in intact rat heart mitochondria utilizing physiological substrates cannot explain respiratory control in vivo.* J Biol Chem, 2011. **286**(35): p. 30816-22.

28. Vinnakota, K.C., et al., *Open-Loop Control of Oxidative Phosphorylation in Skeletal and Cardiac Muscle Mitochondria by Ca(2.).* Biophys J, 2016. **110**(4): p. 954-61.

29. Luongo, T.S., et al., *The Mitochondrial Calcium Uniporter Matches Energetic Supply with Cardiac Workload during Stress and Modulates Permeability Transition.* Cell Rep, 2015. **12**(1): p. 23-34.

30. Kwong, J.Q., et al., *The Mitochondrial Calcium Uniporter Selectively Matches Metabolic Output to Acute Contractile Stress in the Heart.* Cell Rep, 2015. **12**(1): p. 15-22.

31. Lassers, B.W., et al., *Relationship in man between plasma free fatty acids and myocardial metabolism of carbohydrate substrates.* Lancet, 1971. **2**(7722): p. 448-50.

32. Gertz, E.W., et al., *Myocardial substrate utilization during exercise in humans. Dual carbon-labeled carbohydrate isotope experiments.* J Clin Invest, 1988. **82**(6): p. 2017-25.

33. Kuzmiak-Glancy, S. and W.T. Willis, *Skeletal muscle fuel selection occurs at the mitochondrial level.* J Exp Biol, 2014. **217**(Pt 11): p. 1993-2003.

34. LaNoue, K., W.J. Nicklas, and J.R. Williamson, *Control of citric acid cycle activity in rat heart mitochondria.* J Biol Chem, 1970. **245**(1): p. 102-11.

35. Landaw, E.M. and J.J. DiStefano, 3rd, *Multiexponential, multicompartmental, and noncompartmental modeling. II. Data analysis and statistical considerations.* Am J Physiol, 1984. **246**(5 Pt 2): p. R665-77.

36. Nicholls, D.G., S.J. Ferguson, and ScienceDirect (Online service). *Bioenergetics*. 2013, Academic Press, Elsevier: Amsterdam.

37. Dash, R.K. and D.A. Beard, *Analysis of cardiac mitochondrial Na+-Ca2+ exchanger kinetics with a biophysical model of mitochondrial Ca2+ handling suggests a 3:1 stoichiometry.* J Physiol, 2008. **586**(13): p. 3267-85.

38. Dash, R.K., F. Qi, and D.A. Beard, *A biophysically based mathematical model for the kinetics of mitochondrial calcium uniporter.* Biophys J, 2009. **96**(4): p. 1318-32.

39. Eigentler, A., et al., *Laboratory protocol: citrate synthaseamitochondrial marker enzyme*, in *Mitochondrial Physiology Network*. 2015. p. 1-11.

40. Williamson, J.R. and B.E. Corkey, *Assay of citric acid cycle intermediates and related compounds--update with tissue metabolite levels and intracellular distribution.* Methods Enzymol, 1979. **55**: p. 200-22.

Tables

Table 1: Summary of oxygen consumption data

		Leak state	OXPHOS I = 234 nmol min^{-1} (UCS)$^{-1}$		OXPHOS I = 356 nmol min^{-1} (UCS)$^{-1}$	
		J_{O2}	J_{O2}	P/O	J_{O2}	P/O
PYR	$[Ca^{2+}] = 0$	17.1 ± 2.8	55.9 ± 3.7	2.10 ± 0.11	77.3 ± 1.0	2.30 ± 0.02
	$[Ca^{2+}] = 300$ μM	18.7 ± 2.0	58.6 ± 4.7	2.00 ± 0.13	80.9 ± 1.5	2.20 ± 0.03
	$[Ca^{2+}] = 400$ μM	17.8 ± 1.9	58.0 ± 2.9	2.02 ± 0.08	78.4 ± 2.4	2.27 ± 0.06
MIX	$[Ca^{2+}] = 0$	22.2 ± 1.6	62.9 ± 0.6	1.86 ± 0.02	83.0 ± 1.3	2.14 ± 0.03
	$[Ca^{2+}] = 300$ μM	21.4 ± 1.7	61.8 ± 3.1	1.89 ± 0.08	85.1 ± 3.3	2.09 ± 0.07
	$[Ca^{2+}] = 400$ μM	21.5 ± 2.0	62.4 ± 4.4	1.96 ± 0.05	84.7 ± 4.4	2.10 ± 0.09
PC	$[Ca^{2+}] = 0$	21.4 ± 0.9	59.5 ± 4.0	1.88 ± 0.08	77.2 ± 6.2	2.31 ± 0.15
	$[Ca^{2+}] = 300$ μM	21.5 ± 1.1	60.0 ± 4.5	1.87 ± 0.01	80.8 ± 5.0	2.21 ± 0.11
	$[Ca^{2+}] = 400$ μM	20.7 ± 2.4	59.6 ± 1.7	1.96 ± 0.05	78.6 ± 5.8	2.27 ± 0.13

All fluxes reported in units of nmol min^{-1} (UCS)$^{-1}$.

Table 2: Estimated steady-state fluxes

		Leak state fluxes				OXPHOS I = 234 nmol min^{-1} (UCS)$^{-1}$				OXPHOS I = 356 nmol min^{-1} (UCS)$^{-1}$			
		J_1	J_2	J_4	J_{O2}	J_1	J_2	J_4	J_{O2}	J_1	J_2	J_4	J_{O2}
PYR	$[Ca^{2+}] = 0$	11.7±1.8	11.7±4.2	0	17.5±2.0	37.4±2.1	37.2±4.3	0	56.3±3.6	50.9±3.3	49.8±8.1	0	77.4±1.0
	$[Ca^{2+}] = 300$ μM	13.4±2.3	14.3±5.5	0	19.0±1.5	37.2±2.6	33.9±4.9	0	59.2±4.6	52.3±3.6	49.2±9.0	0	81.5±1.5
	$[Ca^{2+}] = 400$ μM	12.4±2.0	12.8±4.8	0	18.2±1.4	39.5±2.6	38.9±5.8	0	59.9±2.9	51.9±3.0	51.1±7.2	0	78.5±2.5
MIX	$[Ca^{2+}] = 0$	6.1±2.7	11.6±1.6	6.3±2.3	22.3±1.2	10.4±4.4	34.3±1.8	24.1±3.7	63.0±0.6	13.1±7.0	42.4±2.3	30.9±5.8	83.1±1.2
	$[Ca^{2+}] = 300$ μM	6.6±2.8	12.0±2.7	5.7±2.3	21.5±1.0	11.4±5.9	31.7±2.2	21.7±5.0	61.9±3.1	23.3±9.8	41.9±2.7	23.0±8.3	85.2±3.3
	$[Ca^{2+}] = 400$ μM	6.3±2.6	10.1±1.3	5.4±2.2	21.7±1.1	14.0±4.7	33.4±1.3	20.2±4.1	62.4±3.4	21.3±9.9	43.4±2.0	25.0±8.6	84.9±4.6
PC	$[Ca^{2+}] = 0$	0	13.2±5.5	11.7±1.8	22.0±0.6	0	29.7±5.6	30.3±2.3	61.1±3.9	0	37.0±9.3	38.4±3.8	78.2±6.2
	$[Ca^{2+}] = 300$ μM	0	11.3±5.8	11.1±1.9	21.5±0.8	0	28.5±5.5	29.7±2.4	60.5±4.5	0	37.6±7.4	39.4±3.0	80.7±5.0
	$[Ca^{2+}] = 400$ μM	0	14.3±6.9	11.7±2.4	20.7±1.7	0	21.9±5.5	27.2±1.9	59.6±1.7	0	36.8±9.9	38.4±4.1	78.4±5.8

All fluxes reported in units of nmol min^{-1} (UCS)$^{-1}$.

Figure Legends

Figure 1: Oxygen fluxes measured by high-resolution respirometry. For all data mitochondria are suspended in a 2-ml Oroboros Oxygraph respirometry chamber at 0.337 U CS per ml. A. Time courses of oxygen consumption rate J_{O2} are shown for buffer total $[Ca^{2+}]$ = 400 μM (with 1 mM EGTA) and three different substrate conditions. Data for t < 0 correspond to the leak state. Infusion of ADP at I = 234 nmol min^{-1} (UCS)$^{-1}$ begins at t = 0 and ends at t = 190 sec. B. Time courses of J_{O2} are shown for $[Ca^{2+}]$ = 400 μM and the three different substrate conditions with ADP infusion rate I = 356 nmol min^{-1} (UCS)$^{-1}$. Infusion begins at t = 0 and ends at t = 125 sec. C. Data on OXPHOS state J_{O2} from N = 3 replicates are shown as Mean ± SEM for three Ca^{2+} concentrations and three different substrate conditions, and for low ATP demand (I = 234 nmol min^{-1} (UCS)$^{-1}$). D. Data on OXPHOS state J_{O2} from N = 3 replicates are shown as Mean ± SEM for three Ca^{2+} concentrations and three different substrate conditions, and for high ATP demand (I = 356 nmol min^{-1} (UCS)$^{-1}$). Abbreviations are PM: pyruvate + malate; MIX: pyruvate + palmitoyl-carnitine + malate; PC: palmitoyl-carnitine + malate.

Figure 2: Time courses of pyruvate and α-ketoglutarate during leak and OXPHOS states for PM (pyruvate + malate) substrate conditions. Straight lines are 25 Monte-Carlo samples representing uncertainty of fits of Eqs. (1) and (2) to the concentration and J_{O2} data. A. Data and model fits are shown for the $[Ca^{2+}]$ = 0 condition, with low ATP demand (I = 234 nmol min^{-1} (UCS)$^{-1}$). B. Data and model fits are shown for the $[Ca^{2+}]$ = 0 condition, with high ATP demand (I = 356 nmol min^{-1} (UCS)$^{-1}$). C. Data and model fits are shown for the $[Ca^{2+}]$ = 300 μM condition, with low ATP demand (I = 234 nmol min^{-1} (UCS)$^{-1}$). D. Data and model fits are shown for the $[Ca^{2+}]$ = 300 μM condition, with high ATP demand (I = 356 nmol min^{-1} (UCS)$^{-1}$). E. Data and model fits are shown for the $[Ca^{2+}]$ = 400 μM condition, with low ATP demand (I = 234 nmol min^{-1} (UCS)$^{-1}$). F. Data and model fits are shown for the $[Ca^{2+}]$ = 400 μM condition, with high ATP demand (I = 356 nmol min^{-1} (UCS)$^{-1}$).

Figure 3: Time courses of pyruvate and α-ketoglutarate during leak and OXPHOS states for MIX (pyruvate + palmitoyl-carnitine + malate) substrate conditions. Straight lines are 25 Monte-Carlo samples representing uncertainty of fits of Eqs. (5) and (6) to the concentration and J_{O2} data. A. Data and model fits are shown for the $[Ca^{2+}]$ = 0 condition, with low ATP demand (I = 234 nmol min^{-1} (UCS)$^{-1}$). B. Data and model fits are shown for the $[Ca^{2+}]$ = 0 condition, with high ATP demand (I = 356 nmol min^{-1} (UCS)$^{-1}$). C. Data and model fits are shown for the $[Ca^{2+}]$ = 300 μM condition, with low ATP demand (I = 234 nmol min^{-1} (UCS)$^{-1}$). D. Data and model fits are shown for the $[Ca^{2+}]$ = 300 μM condition, with high ATP demand (I = 356 nmol min^{-1} (UCS)$^{-1}$). E. Data and model fits are shown for the $[Ca^{2+}]$ = 400 μM condition, with low ATP demand (I = 234 nmol min^{-1} (UCS)$^{-1}$). F. Data and model fits are shown for the $[Ca^{2+}]$ = 400 μM condition, with high ATP demand (I = 356 nmol min^{-1} (UCS)$^{-1}$).

Figure 4: Time courses of pyruvate and α-ketoglutarate during leak and OXPHOS states for PC (palmitoyl-carnitine + malate) substrate conditions. Straight lines are 25 Monte-Carlo samples representing uncertainty of fits of Eqs. (3) and (4) to the concentration and J_{O2} data. A. Data and model fits are shown for the $[Ca^{2+}]$ = 0 condition, with low ATP demand (I = 234 nmol min^{-1} (UCS)$^{-1}$). B. Data and model fits are shown for the $[Ca^{2+}]$ = 0 condition, with high ATP demand (I = 356 nmol min^{-1} (UCS)$^{-1}$). C. Data and model fits are shown for the $[Ca^{2+}]$ = 300 μM condition, with low ATP demand (I = 234 nmol min^{-1} (UCS)$^{-1}$). D. Data and model fits are shown for the $[Ca^{2+}]$ = 300 μM condition, with high ATP demand (I = 356 nmol min^{-1} (UCS)$^{-1}$). E. Data and model fits are shown for the $[Ca^{2+}]$ = 400 μM condition, with low ATP demand (I = 234 nmol min^{-1} (UCS)$^{-1}$). F. Data and model fits are shown for the $[Ca^{2+}]$ = 400 μM condition, with high ATP demand (I = 356 nmol min^{-1} (UCS)$^{-1}$).

Figure 5: Quasi-steady-state TCA cycle fluxes. Definitions of steady-state fluxes used in the quasi-steady analysis of Eqs. (1)-(5) are illustrated. The major assumptions are that rates of change bulk concentrations of citrate, isocitrate, succinyl-CoA, succinate, fumarate, and oxaloacetate are much smaller in magnitude than rates of change of pyruvate, fatty acid, α-ketoglutarate, and malate.

Figure 6: Predicted flux distribution for mixed substrate conditions. The diagrams shows predicted values of steady fluxes at different calcium concentrations for the high ATP demand (I = 356 nmol min^{-1} (UCS)$^{-1}$) case. Pyruvate dehydrogenase flux increases and β-oxidation flux decreases as $[Ca^{2+}]$ is increased. Fluxes are reported in units of nmol min^{-1} (UCS)$^{-1}$ and as maximally likelihood ± one standard deviation.

Figure 7: Mitochondrial fuel selection. A. Fractional oxidation of pyruvate versus palmitoyl-carnitine is plotted as a function of total $[Ca^{2+}]$ under the low ATP demand (I = 234 nmol min^{-1} $(UCS)^{-1}$) condition. The observed trend of increasing fractional utilization of pyruvate with increasing $[Ca^{2+}]$ is not statistically significant, with estimated p = 0.28. B. Fractional oxidation of pyruvate versus palmitoyl-carnitine is plotted as a function of total $[Ca^{2+}]$ under the high ATP demand (I = 356 nmol min^{-1} $(UCS)^{-1}$) condition. The observed trend of increasing fractional utilization of pyruvate with increasing $[Ca^{2+}]$ is not statistically significant, with estimated p = 0.19.

Figure 8: Calcium control of mitochondrial fuel selection. Estimate fraction utilization of pyruvate is shown for low- and high-ATP demand conditions (I = 234 and 356 nmol min^{-1} $(UCS)^{-1}$) with zero calcium and with non-zero calcium. The non-zero calcium estimates are obtained by combining data from total $[Ca^{2+}]$ = 300 and 400 μM cases.

Figure 9: Estimated leak current. The leak current J_L is plotted as a function of ATP demand. Estimates are obtained by combining data for all substrate conditions. (No substrate-dependent differences in J_L were detected.) Leak current is highest in the leak state (ATP demand I = 0) and decreases as ATP demand is increased.

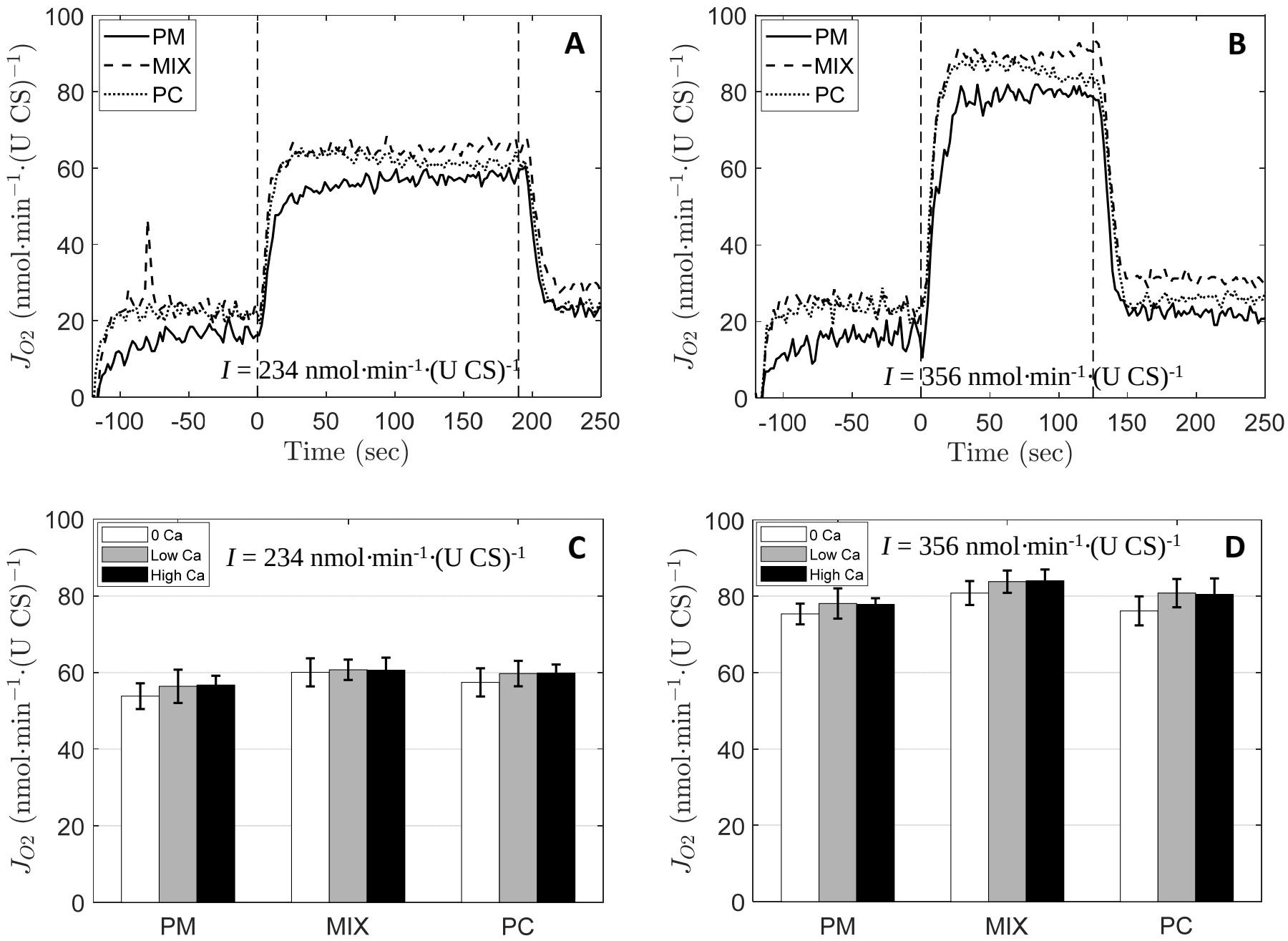
A
PM
MIX
PC
I = 234 nmol·min-1·(U CS)-1
Time (sec)
B
I = 356 nmol·min-1·(U CS)-1
C
0 Ca
Low Ca
High Ca
D
PM
MIX
PC

Figure 1

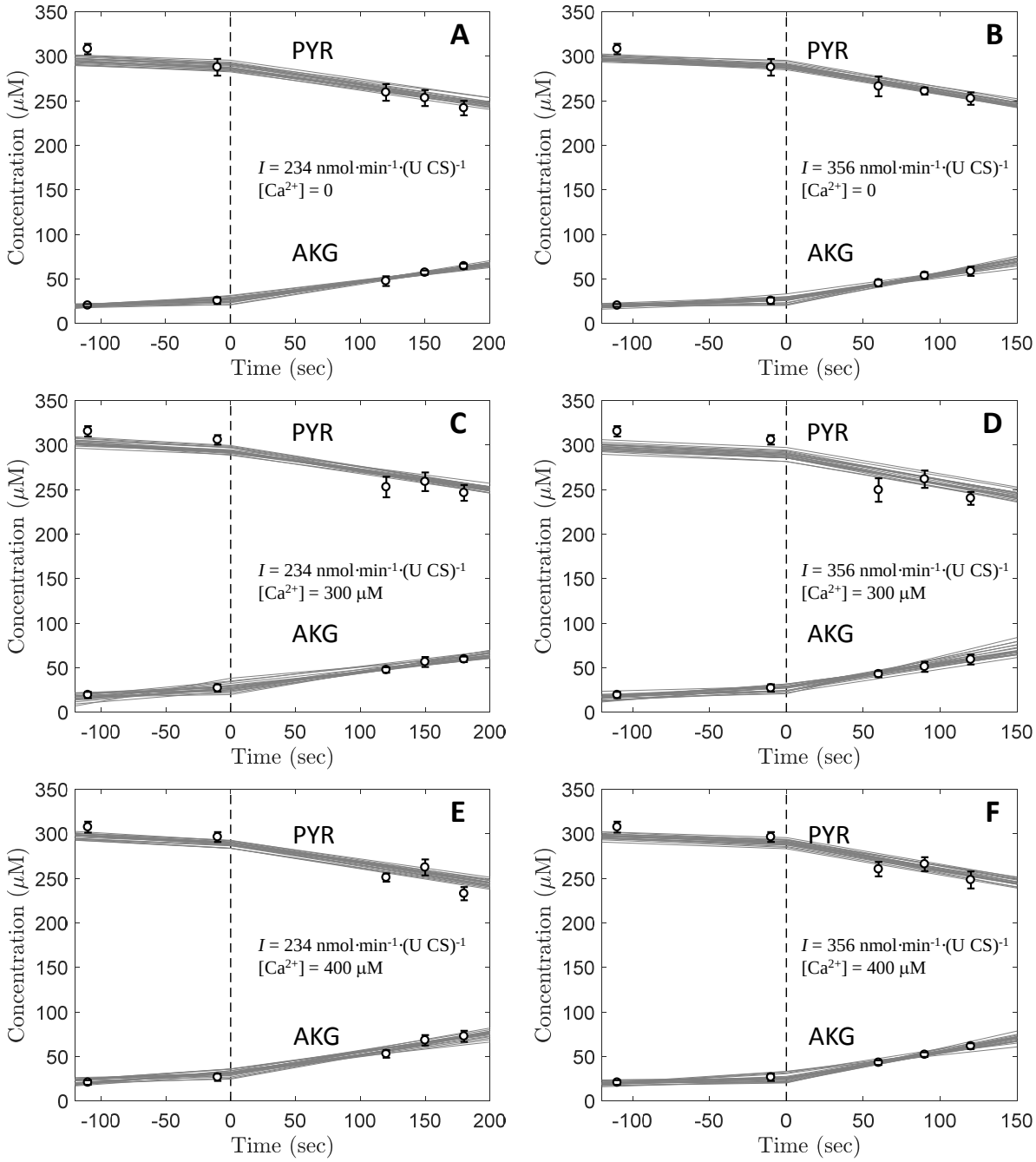
A
PYR
AKG
I = 234 nmol·min-1·(U CS)-1
[Ca2+] = 0
B
PYR
AKG
I = 356 nmol·min-1·(U CS)-1
[Ca2+] = 0
C
PYR
AKG
I = 234 nmol·min-1·(U CS)-1
[Ca2+] = 300 μM
D
PYR
AKG
I = 356 nmol·min-1·(U CS)-1
[Ca2+] = 300 μM
E
PYR
AKG
I = 234 nmol·min-1·(U CS)-1
[Ca2+] = 400 μM
F
PYR
AKG
I = 356 nmol·min-1·(U CS)-1
[Ca2+] = 400 μM
Concentration (μM)
Time (sec)

Figure 2

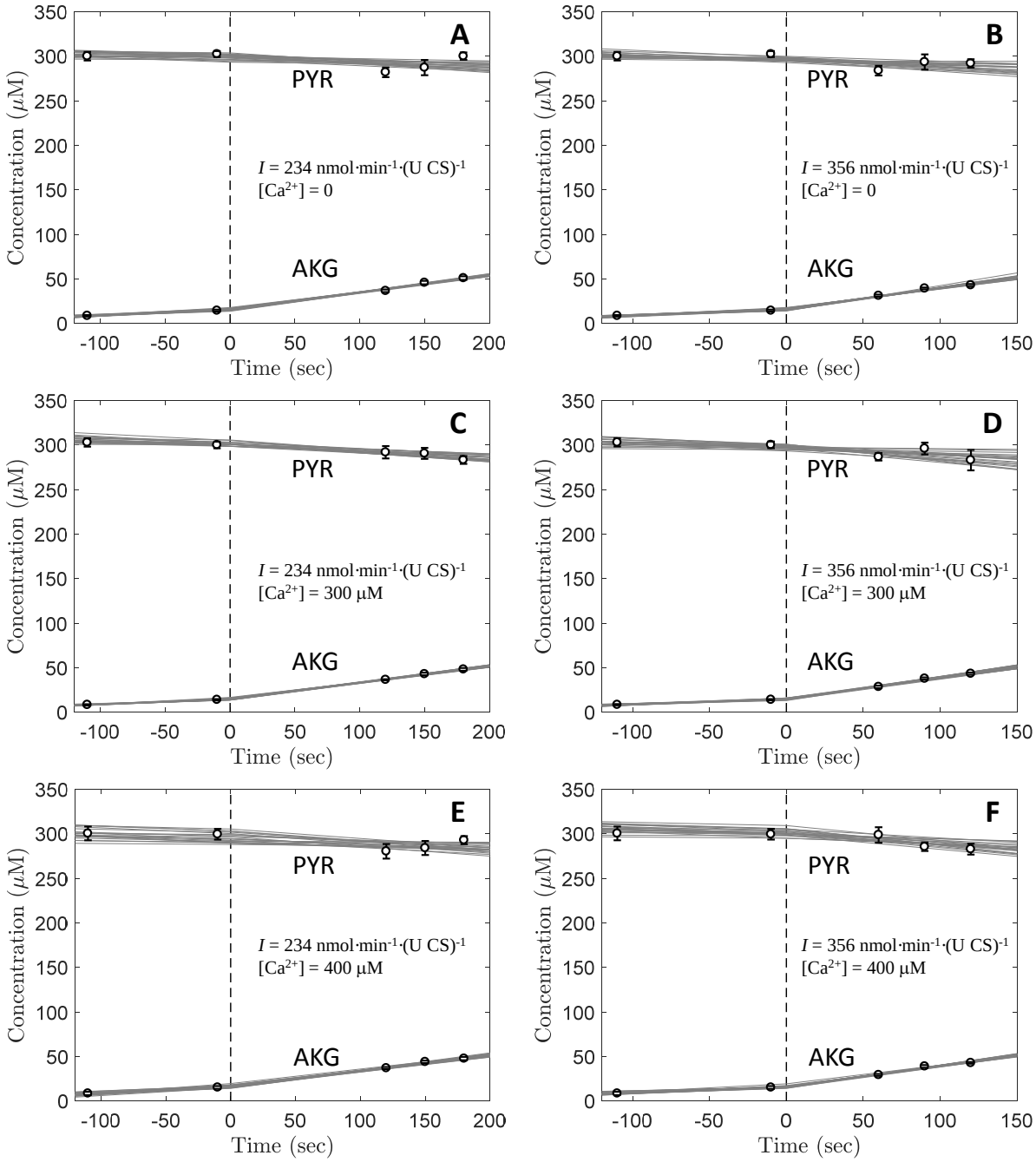
A
PYR
AKG
I = 234 nmol·min-1·(U CS)-1
[Ca2+] = 0
B
PYR
AKG
I = 356 nmol·min-1·(U CS)-1
[Ca2+] = 0
C
PYR
AKG
I = 234 nmol·min-1·(U CS)-1
[Ca2+] = 300 μM
D
PYR
AKG
I = 356 nmol·min-1·(U CS)-1
[Ca2+] = 300 μM
E
PYR
AKG
I = 234 nmol·min-1·(U CS)-1
[Ca2+] = 400 μM
F
PYR
AKG
I = 356 nmol·min-1·(U CS)-1
[Ca2+] = 400 μM
Concentration (μM)
Time (sec)

Figure 3

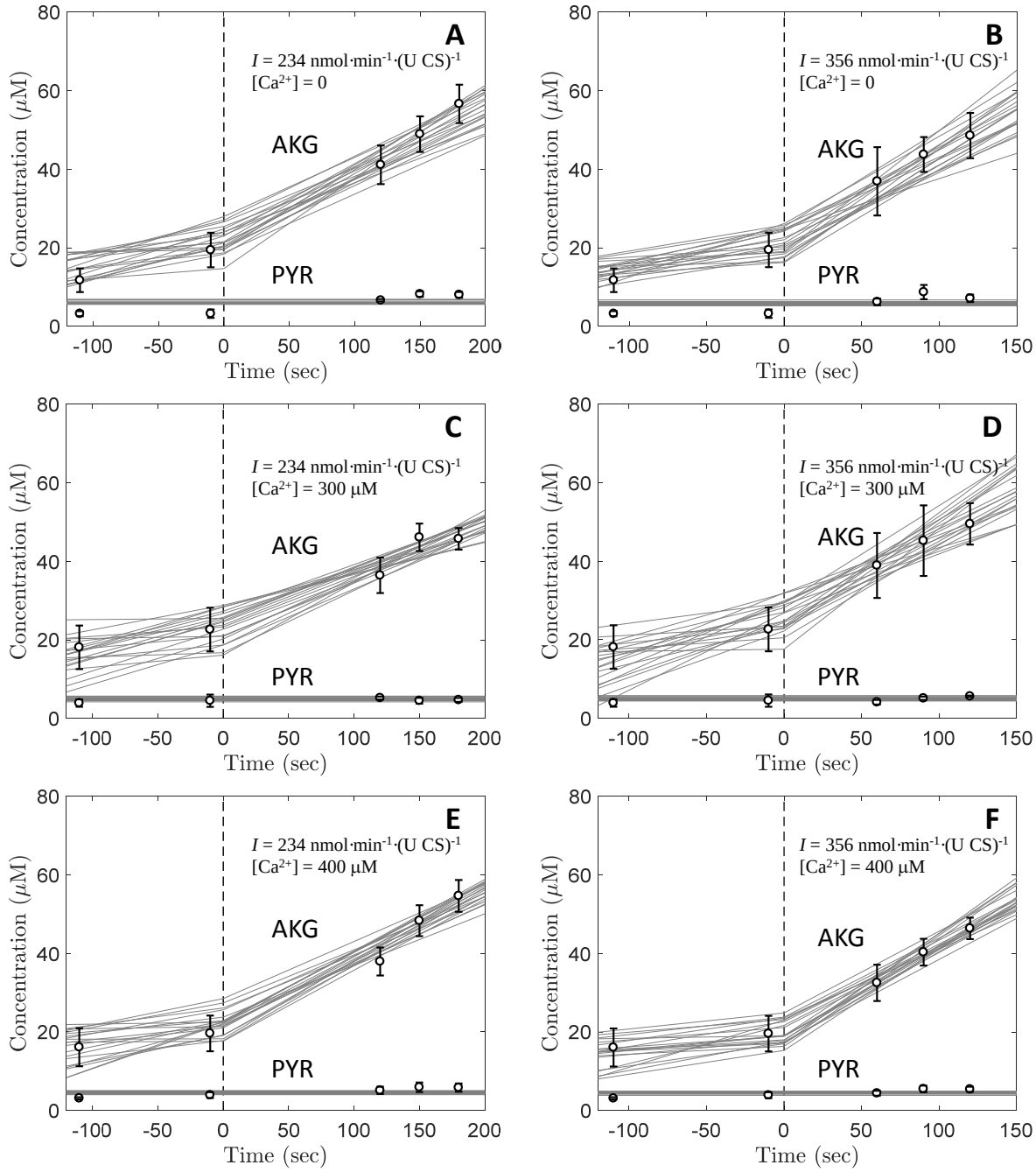
A
I = 234 nmol·min-1·(U CS)-1
[Ca2+] = 0
AKG
PYR
B
I = 356 nmol·min-1·(U CS)-1
[Ca2+] = 0
AKG
PYR
C
I = 234 nmol·min-1·(U CS)-1
[Ca2+] = 300 μM
AKG
PYR
D
I = 356 nmol·min-1·(U CS)-1
[Ca2+] = 300 μM
AKG
PYR
E
I = 234 nmol·min-1·(U CS)-1
[Ca2+] = 400 μM
AKG
PYR
F
I = 356 nmol·min-1·(U CS)-1
[Ca2+] = 400 μM
AKG
PYR
Concentration (μM)
Time (sec)

Figure 4

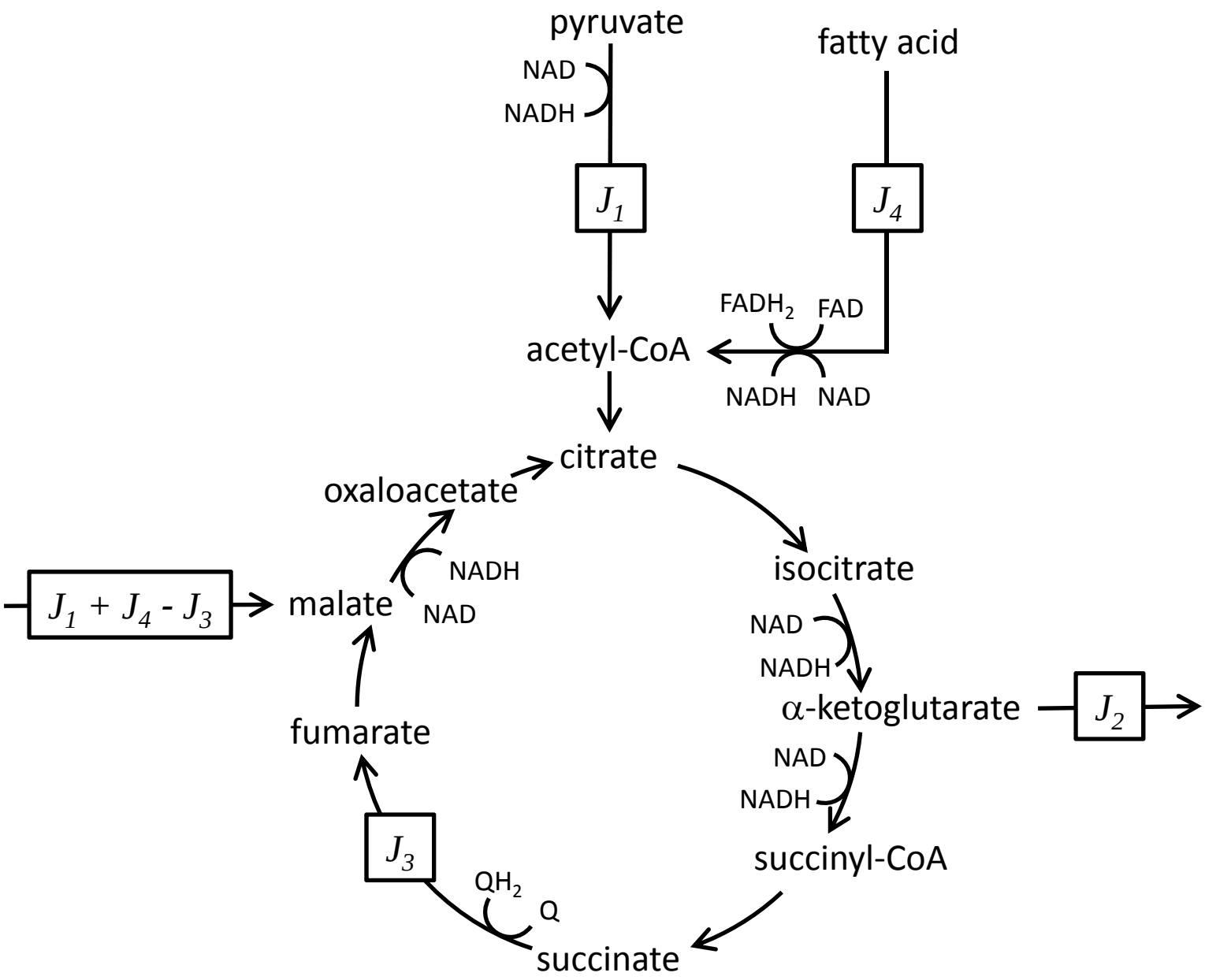
pyruvate
NAD
NADH
J_1
fatty acid
J_4
$FADH_2$
FAD
acetyl-CoA
NADH
NAD
citrate
oxaloacetate
NADH
NAD
$J_1 + J_4 - J_3$
malate
isocitrate
NAD
NADH
α-ketoglutarate
J_2
NAD
NADH
succinyl-CoA
fumarate
J_3
QH_2
Q
succinate

Figure 5

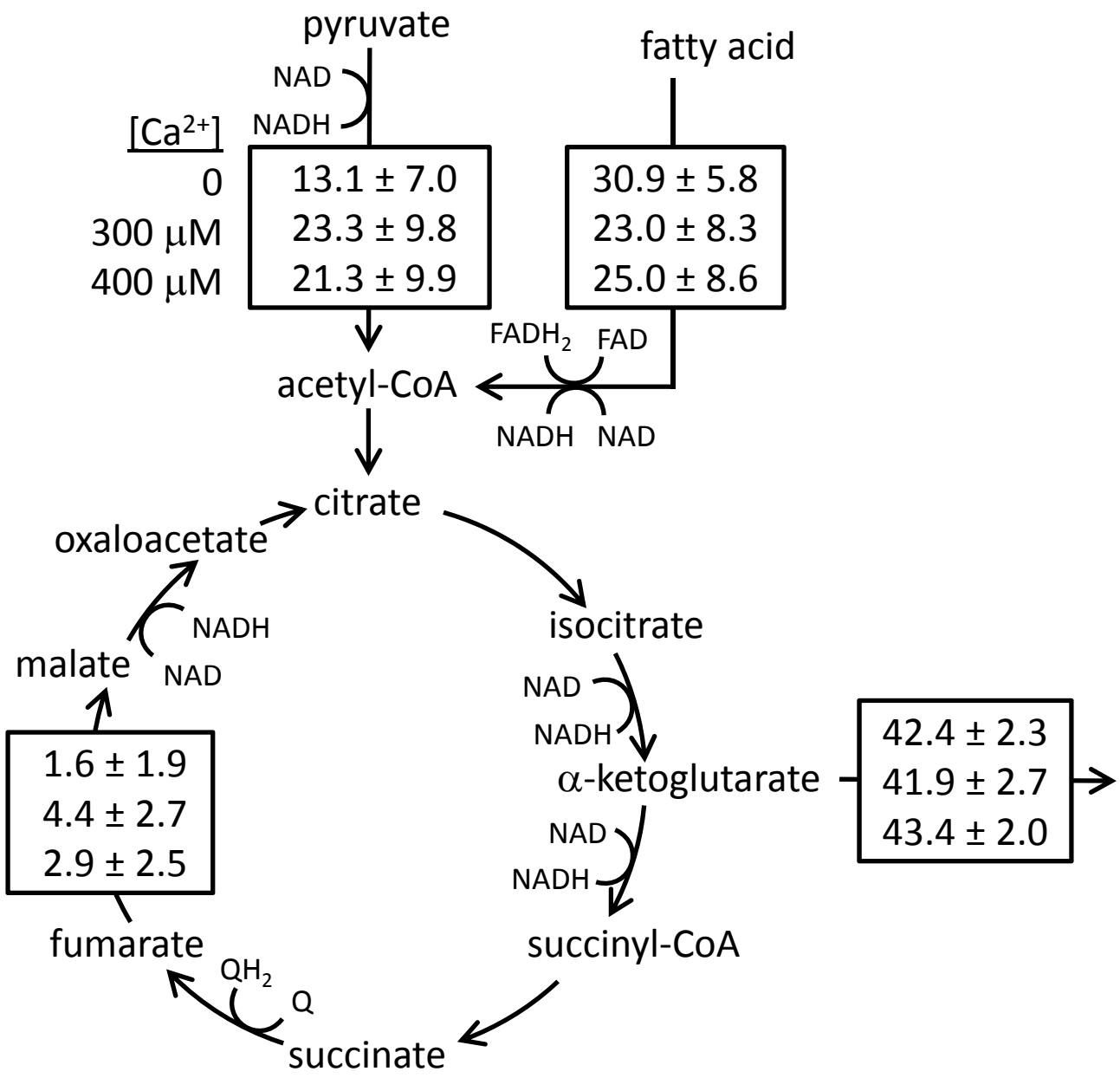
pyruvate
NAD
NADH
fatty acid
[Ca2+]
0
300 μM
400 μM
13.1 ± 7.0
23.3 ± 9.8
21.3 ± 9.9
30.9 ± 5.8
23.0 ± 8.3
25.0 ± 8.6
FADH2
FAD
acetyl-CoA
NADH
NAD
citrate
oxaloacetate
isocitrate
NADH
malate
NAD
NAD
NADH
α-ketoglutarate
42.4 ± 2.3
41.9 ± 2.7
43.4 ± 2.0
1.6 ± 1.9
4.4 ± 2.7
2.9 ± 2.5
NAD
NADH
fumarate
succinyl-CoA
QH2
Q
succinate

Figure 6

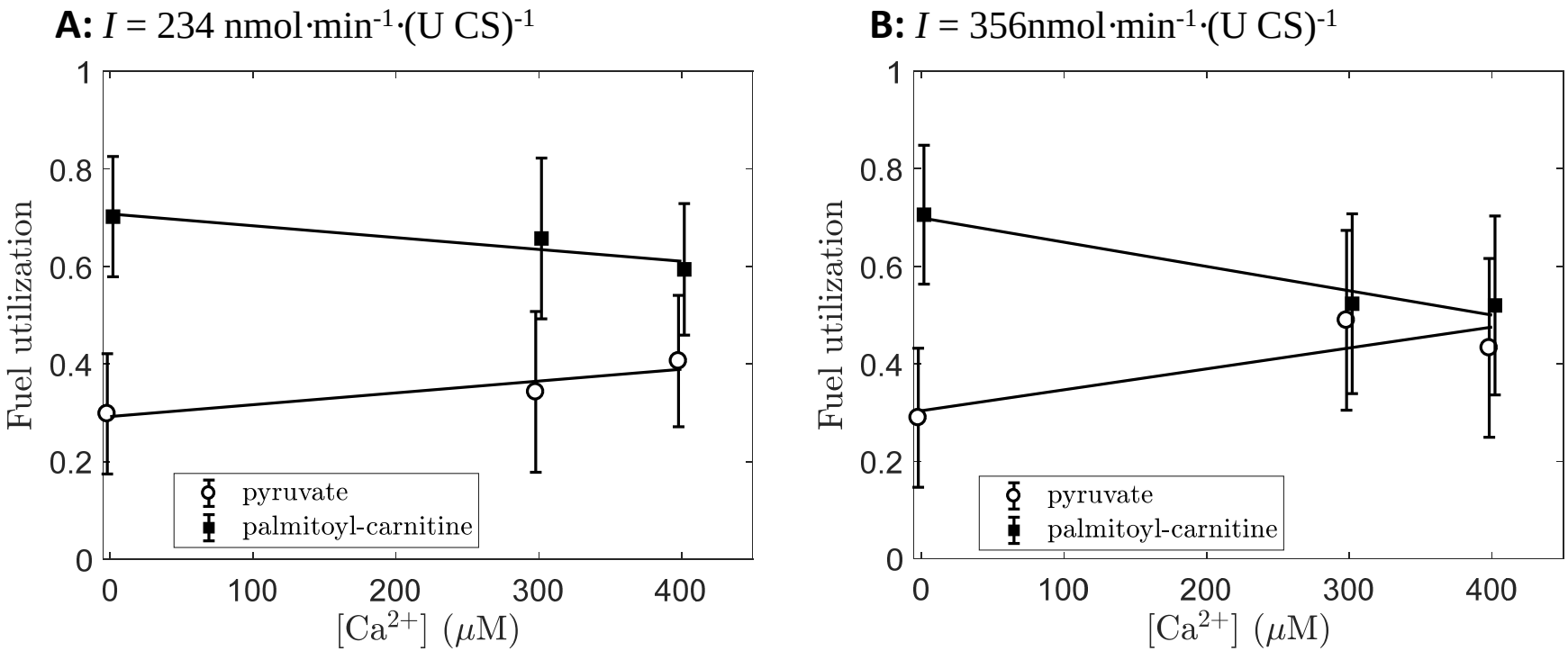
A: I = 234 nmol·min-1·(U CS)-1
B: I = 356nmol·min-1·(U CS)-1
Fuel utilization
[Ca2+] (μM)
pyruvate
palmitoyl-carnitine
0
0.2
0.4
0.6
0.8
1
0
100
200
300
400

Figure 7

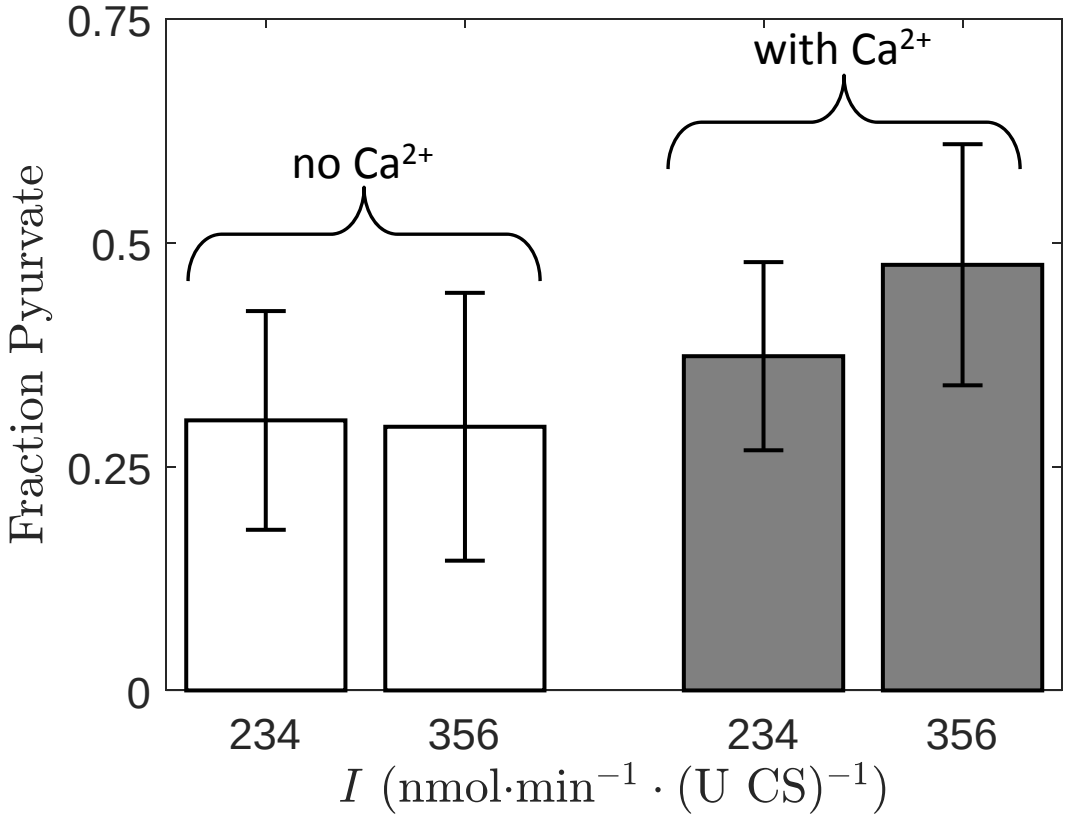
0.75
0.5
0.25
0
Fraction Pyurvate
no Ca2+
with Ca2+
234
356
234
356
I (nmol·min−1 · (U CS)−1)

Figure 8

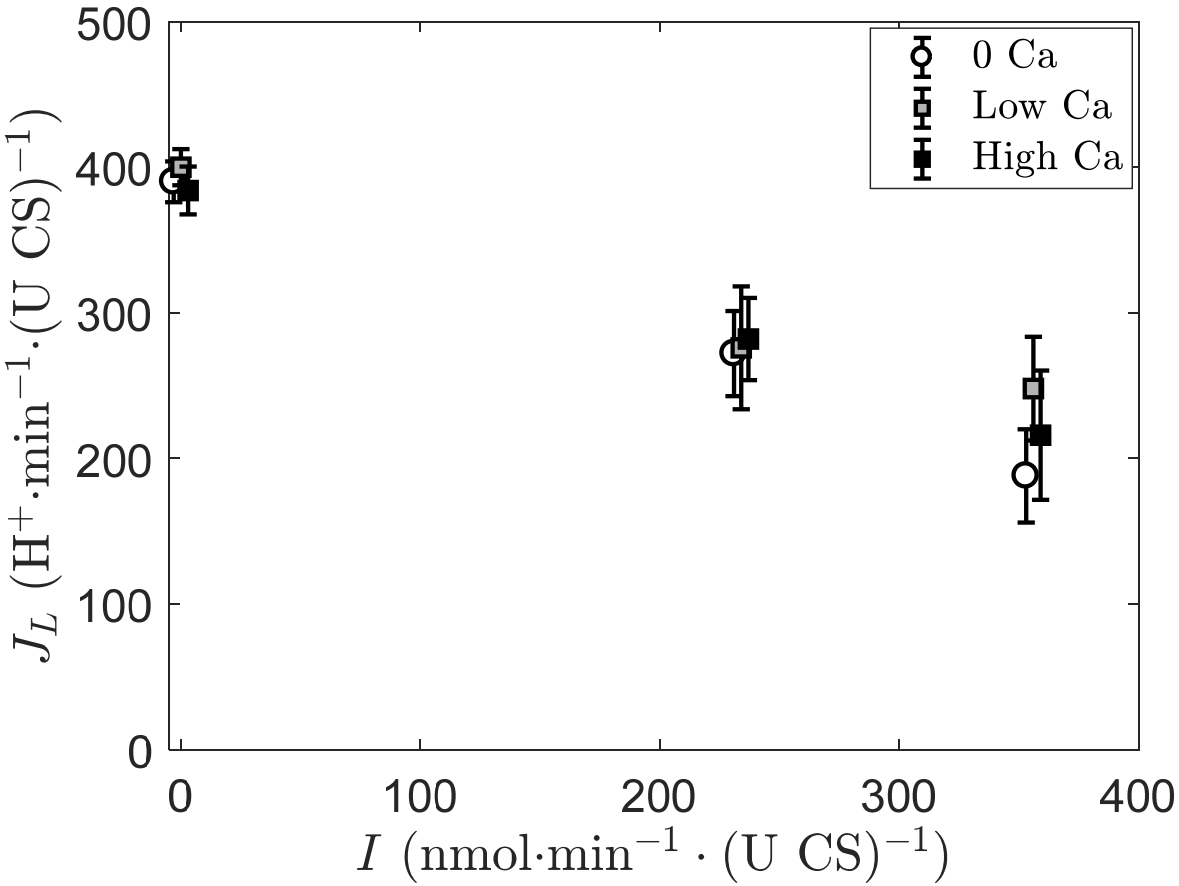
0 Ca
Low Ca
High Ca
500
400
300
200
100
0
0
100
200
300
400
J_L (H$^+$·min^{-1}·(U CS)$^{-1}$)
I (nmol·min^{-1} · (U CS)$^{-1}$)

Figure 9